THE ASTROPHYSICAL JOURNAL, 473:533–538, 1996 December 10

RECONNECTION AND HELICITY IN A SOLAR FLARE

ALEXEI A. PEVTSOV AND RICHARD C. CANFIELD
Institute for Astronomy, University of Hawaii, 2680 Woodlawn Drive, Honolulu, HI 96822; apevtsov@solar.stanford.edu
AND
HAROLD ZIRIN
Big Bear Solar Observatory, California Institute of Technology, Pasadena, CA 91125
Received 1996 April 15; accepted 1996 June 28

ABSTRACT

Using X-ray images, Hα images, and vector magnetograms, we have studied the evolution of the coronal structure and magnetic field of NOAA Active Region 7154 during 1992 May 5–12. A two-ribbon 4B/M7.4 flare associated with an Hα filament eruption was observed on May 8, 15:13–19:16 UT. An interesting feature of the region was a long, twisted X-ray structure, which formed shortly before the flare and disappeared after it, being replaced by a system of unsheared postflare loops. Neither the X-ray nor Hα morphology nor the photospheric magnetic field shows any indication of gradual buildup of nonpotential energy prior to the flare. Rather, the long structure appears to result from the reconnection of two shorter ones just tens of minutes before the filament eruption and flare.

Using vector magnetograms and X-ray morphology, we determine the helicity density of the magnetic field using the force-free field parameter α. The observations show that the long structure retained the same helicity density as the two shorter structures, but its greater length implies a higher coronal twist. The measured length and α value combine to imply a twist that exceeds the threshold for the MHD kink instability in a force-free cylindrical flux tube. We conclude that theoretical studies of such simple models, which have found that the MHD kink instability does not lead to global dissipation, do not adequately address the physical processes that govern coronal magnetic fields.

Subject headings: MHD — Sun: corona — Sun: flares — Sun: magnetic fields — Sun: X-rays, gamma rays

1. INTRODUCTION

It is well documented that magnetic reconnection plays a key role in flare energy release, and *Yohkoh* observations have shown that many flares are well represented by the classical flare model of eruption followed by reconnection (see Tsuneta 1996; Švestka & Cliver 1992). *Yohkoh* observations show that ejecta are common feature of flares—even of compact hard X-ray flares (Shibata et al. 1995). *Yohkoh* observations also suggest that reconnection plays a role in other eruptive phenomena. Feynman & Martin (1995) showed that eruptions of filaments are most likely to occur when new flux emerges nearby in an orientation favorable for reconnection. Both flares and filaments are thought to be associated with twisted magnetic fields (e.g., Moore & Roumeliotis 1992; van Ballegooijen & Martens 1990).

Some authors (e.g., Priest 1984; Roumeliotis, Sturrock, & Antiochos 1994) have shown theoretically that flux tubes will become unstable because of shear motions of footpoints. Hanaoka (1994) inferred shear from sunspot motions. Rotational motions of flux-tube endpoints will also introduce twist and lead to instability (e.g., Priest 1984). Sunspots occasionally show rotational motions (e.g., Druzhinin et al. 1993, and references therein). However, in a specific study of two sunspots, we found no clear correlation between variations of magnetic helicity and rotational motions (Pevtsov, Canfield, & Metcalf 1995, hereafter Paper II). In no case with which we are familiar is it compellingly demonstrated that either shear or rotational motions cause chromospheric or coronal eruptions.

It has been shown that a simple magnetic flux tube is linearly unstable to kinking if the twist from one end to the other exceeds a critical value Φ_c (e.g., Priest 1984). Hood & Priest (1979) estimated that for a monotonically twisted force-free field $\Phi_c = 2.5\pi$. In an observational study of 28 prominences that showed helical patterns, Vrsnak, Ruzdjak, & Rompolt (1991) found that eruptive prominences show higher observed twist than quiet ones. No observed prominence had a value of twist exceeding 2π. Thus, it seems reasonable to believe that magnetic flux tubes in the solar atmosphere become globally unstable to kinking at about this value of Φ. If shear or rotational motions of the footpoints do not play a role in destabilizing filaments, can reconnection do so?

We analyze the early stages of the coronal evolution of NOAA Active Region (AR) 7154, where a large flare was observed. An interesting feature of this flare was a beautiful inverse-*S* coronal structure that formed shortly before the flare began. In general, the shape of coronal loops is a signature of the helicity of their magnetic fields—i.e., *S*-shaped loops match flux tubes of positive current helicity, and inverse-*S*–shaped loops match flux tubes of negative current helicity (e.g., Canfield, Pevtsov, & Acton 1995). In this paper, we study in detail the formation of the inverse *S* coronal loop of AR 7154, in order to understand the role of MHD instability in this eruption. In § 2, we describe the observational data we used: Haleakala Stokes Polarimeter vector magnetograms, *Yohkoh* Soft X-Ray Telescope observations, and Hα observations from Big Bear Solar Observatory. In § 3, we sketch the morphological evolution of the coronal loops above the active region, as well as their magnetic field and helicity. Our observations imply that an unstable coronal loop was created because of reconnection and the consequent formation of a loop whose twist exceeded Φ_c.

2. INSTRUMENTATION AND DATA REDUCTION

The two-ribbon 4B/M7.4 flare of 1992 May 8, 1513 UT occurred at S25 E07 in NOAA AR 7154, which we observed from May 5–12 (S25 E42-W46) with the Mees Solar Observatory Haleakala Stokes Polarimeter (Mickey 1985) and the *Yohkoh* Soft X-ray Telescope (SXT) (Tsuneta et al. 1991). On May 8, we also observed the flare itself using the Hα telescopes of Big Bear Solar Observatory (BBSO). The magnetograms and X-ray images were coaligned to an accuracy of a few arcseconds using sunspots in white images.

The Haleakala Stokes Polarimeter data set consists of 19 magnetograms obtained on seven observing days. The instrument uses a 6″ circular aperture and scans the solar image to build up a vector magnetogram. We used the two standard types of vector magnetograms (Canfield et al. 1993), i.e., half resolution (spatial step 5.″6) and full resolution (spatial step 2.″8). The magnetograms were derived from Stokes profiles of the spectral lines Fe I λλ6301.5 and 6302.5, using the nonlinear least-squares Unno-profile–fitting routine of Skumanich & Lites (1987). The method makes a first-order correction for magneto-optical and magnetic filling factor effects.

For each magnetogram, we resolved the 180° azimuthal ambiguity of the transverse field $B_{\rm trans}$ following Canfield et al. (1993). The noise level in the original magnetograms is about 70 G for $B_{\rm trans}$ and 10 G for $B_{\rm long}$. We computed maps of the horizontal distribution of the force-free field parameter $\alpha(x, y)$ from the vertical (z) component of $\nabla \times \boldsymbol{B} = \alpha \boldsymbol{B}$, as in Pevtsov, Canfield, & Metcalf (1994, hereafter Paper I). For each magnetogram, we also computed linear force-free fields following Gary (1989). We determined the best single value $\alpha_{\rm best}$ for the active region as a whole by minimizing the difference between the x and y components of the computed constant-α force-free and observed horizontal magnetic fields, using only those highly significant pixels for which $B_{\rm trans} > 300$ G. Both $\alpha(x, y)$ and $\alpha_{\rm best}$ measure the density of current helicity (Papers I and II) and twist.

Partial-frame SXT images were used to study evolution of coronal structures before and after the flare. The images have 2.″46 pixels and are taken every 2 s using Al.1 and Al12 (thin and thick aluminum) filters in succession. Because of satellite night, observations were not made during the main phase of the flare, between 15:08 UT and 15:43 UT.

The BBSO Hα observations were started at 15:02 UT—about 10 minutes before the flare began—and continued until 18:56 UT in Hα and both wings (±0.6 Å), as well as the K line and videomagnetograph, using both 25 and 65 cm telescopes. The time resolution of the Hα observations was about 20 s.

3. ACTIVE REGION STRUCTURE AND EVOLUTION

The interesting features of this region included the formation of a long inverse-*S* structure seen in X-rays (§ 3.1) and a filament eruption seen in Hα preceding the flare (§ 3.2). However, the region as a whole showed no systematic buildup of magnetic shear (§ 3.3).

3.1. *Formation of the Long Inverse S Structure*

The SXT observations of May 5–8 show high loops arching over the whole region, which are rooted in magnetic fields on the outer boundary of the active region, and lower

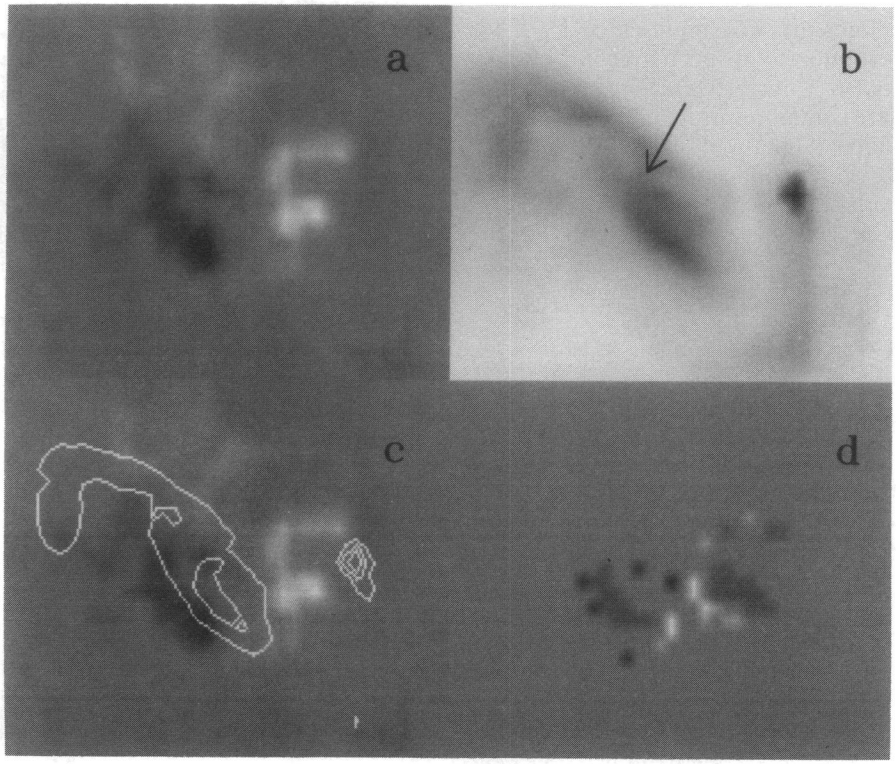

FIG. 1.—Overview of NOAA AR 7154 on 1992 May 6 with a 226″ × 170″ field of view. (*a*) Vertical field magnetogram, 19:09 UT, 5.″6 pixel size (*white means positive polarity*); (*b*) X-ray image, 23:31 UT, Al.1 (thin aluminum) filter, with a 2.″46 pixel size. Arrow indicates gap between two separate loops. (*c*) Coregistered X-ray image contours superposed on magnetogram (*a*). (*d*) Maps of the force-free field parameter α, ranging from -5×10^{-7} m^{-1} (*black*) to $+5 \times 10^{-7}$ m^{-1} (*white*). Solar north is up in all figures except Fig. 3.

lying loops, which connect to the stronger (inner) magnetic fields. The latter loops are the subject of our interest here. Figure 1*a* shows the underlying photospheric magnetic field. Figure 1*b* shows an SXT X-ray image. The overlay in Figure 1*c* shows how the two are related. In the northeastern part of the region, loops connect the back of the leading polarity with the back of the following polarity in the shape of a fishhook (inverse-*J* shaped). In the southwestern part of the region, other loops connect the front of the following polarity with the front of the leading polarity, also with a fishhook shape. Together, these two fishhook-shaped structures nearly join to form an "inverse-*S*–shaped" structure—though it is discontinuous in the middle—like the arms of a barred spiral galaxy. This cut inverse-*S* structure was seen for 3 days of observations before the flare. The location of the cut on May 6, two days before the flare, is shown by the arrow in Figure 1*b*.

The α map shows values only where they can be unambiguously determined in the presence of noise. The overall background (*gray*) indicates that no significant value can be determined; darker gray indicates negative α values, and lighter gray indicates positive values. The predominant sign of α is negative, in agreement with the inverse-*S* shape of the coronal structures and α_{best}. However, patches of both signs are seen, with amplitudes much different from $|\alpha_{best}|$. The wide range of α values in an active region is not uncommon (Paper I).

Important changes occurred prior to the flare. At about 21 UT on May 7, the day before the flare, the *Yohkoh* observations show that short bright loops started to develop in the cut part of the inverse *S*. Gradually these new loops filled the space between the footpoints of the loops rooted in the leading and following polarity. However, the cut inverse *S* did not change significantly in curvature or topology until tens of minutes before the flare, when the two parts united in one continuous long structure. Figure 2 shows SXT images during the 30 minute period that led to the formation of a bright uncut inverse-*S* structure by 15:01:40 UT (see Fig. 2*d*). The arrow in Figure 2*b* shows the cut and a short bright loop within it, immediately to the right of the head of the arrow. According to Solar Geophysical Data (1992), the X-ray flare began at 15:13 UT. The large inverse-*S* loop disappeared after the flare, although the general coronal structure of the region (but no single structure) continued to show inverse-*S* form (*faint outer part*, Fig. 2*f*). During the decay phase of the flare, an arcade of postflare loops was clearly evident (Moore et al. 1980).

3.2. *Filament Eruption*

BBSO images show two Hα filaments, with one lying under each of the two fishhook X-ray structures. Together they also form an overall inverse-*S* shape, but there is a cut in the inverse *S* due to a gap between the two filaments.

On May 7 and 8, small sunspots drifted into this gap. This is the most direct evidence of photospheric magnetic field changes. A few field-transition arches are seen, but no arch filament system is evident.

The first BBSO observations on May 8—in both blue wings and red wings of Hα—were made at 15:01:50 UT, about 12 minutes before the Hα flare began. The northeast filament was already activated—indicated by strong absorption in both wings—presumably because of unwinding or other internal motions. Also, the structure was bright in X-rays (Fig. 2*d*) at this time.

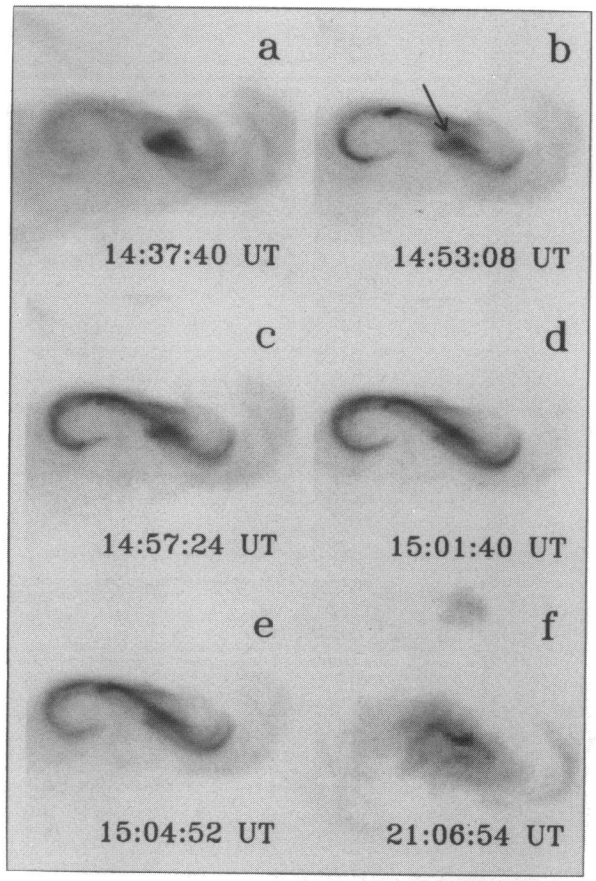

FIG. 2.—Sequence of *Yohkoh* SXT images showing the development of the inverse-*S* loop before the flare of 1992 May 8 15:12 UT. Each frame, obtained with the A1.1 (thin aluminium) filter, has a 314″ × 314″ field of view and 2.″46 × 2.″46 pixels. (*a*) UT = 14:37:40; (*b*) UT = 14:53:08; (*c*) UT = 14:57:24; (*d*) UT = 15:01:40; (*e*) UT = 15:04:52; (*f*). After the flare on May 9, UT = 21:06:54.

Figure 3 (rotated 180° relative to all other figures) shows clear evidence for eruption of the filament. The 15:02:35 (blue wing) and 15:02:38 UT (red wing) images show filament absorption in both wings. The 15:13:53 UT image and earlier image show an eastward proper motion, and that a filament layer has split off. The first flare brightenings are seen at this time. Between 15:19:10 and 16:14:58 UT the flare ribbons spread very significantly. At 16:14:58 UT, both postflare loops and a residual inversion line filament can be seen. This eruption is an example of a type called a filament layer eruption, in which a layer of a filament erupts but part of the filament remains. Filament layer eruptions were first described by Tang (1986).

3.3. *Lack of Evidence for Gradual Buildup of Shear*

In search of evidence of gradual buildup that might be associated with the overall (large-scale) twisted structure of the active region, we examined the variation of α_{best} for several days around the time of the flare. Figure 4 shows the observed variation of this measure of the average helicity density derived from all 19 Haleakala Stokes Polarimeter vector magnetograms. The time-averaged value of α_{best} was -2.25 ± 0.10, in units of 10^{-8} m^{-1}. The individual values of α_{best} shows no significant variations on daily timescales. Our α maps are coarse, and we cannot exclude the possibility that shear build up occurs at unresolved scales. However, we consider it unlikely that such buildup would

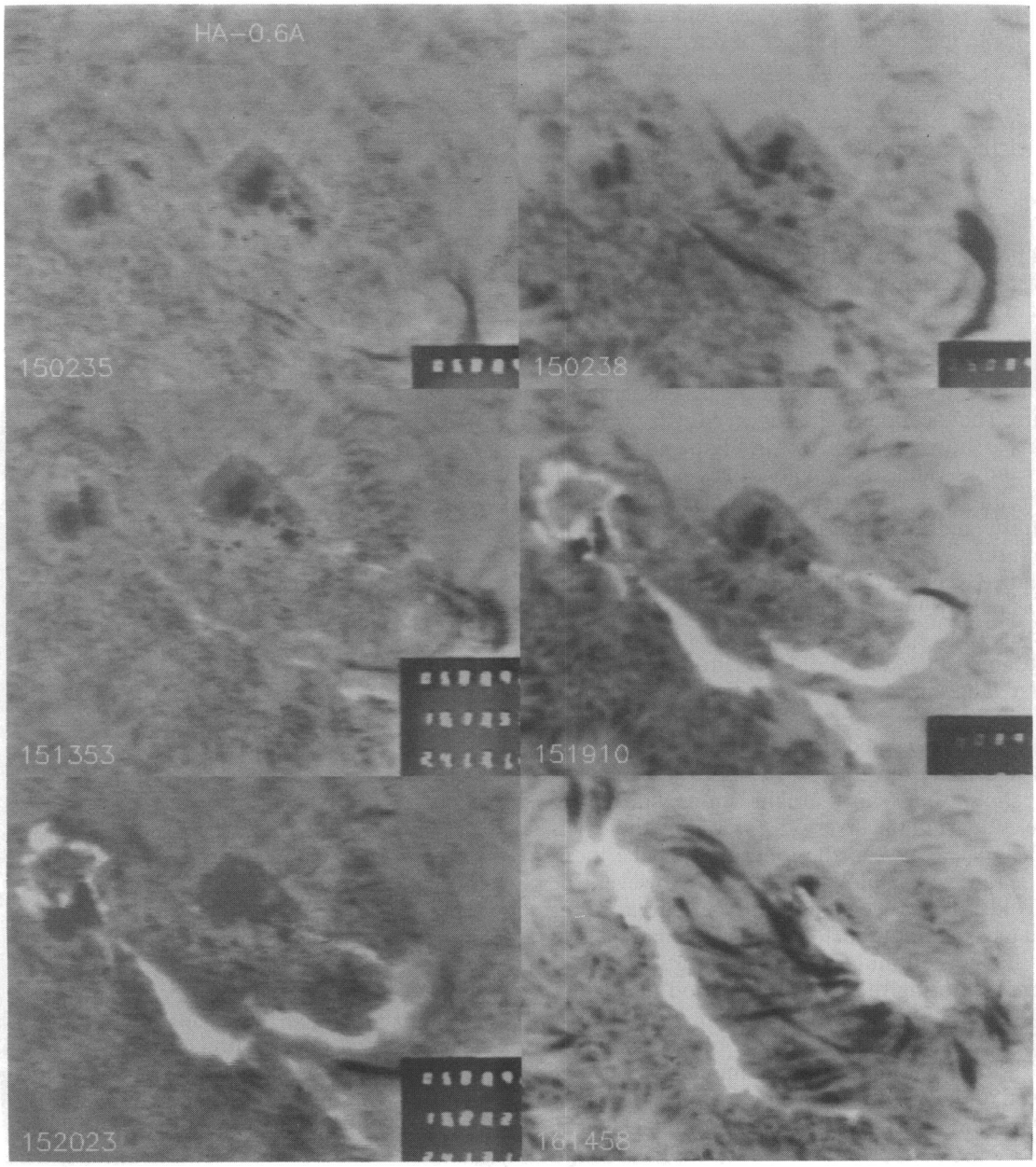

FIG. 3.—BBSO Hα blue wing (*left*) and red wing (*right*) images of the filament eruption and flare of 1992 May 8. East-west field of view is approximately 150″. Terrestrial north is down, and east is to the right.

have no manifestations on observable scales. Therefore, we conclude that gradual buildup of shear by evolutionary motion on timescales of days does not provide a viable explanation for the occurrence of this flare, which leads us to consider the role of reconnection.

4. INTERPRETATION

Our interpretation of the sequence of SXT images shown in Figure 2 is that a long, single inverse *S* coronal structure was formed by reconnection of two existing shorter loops that were parts of the cut inverse-*S* structure earlier. Two observations suggest that this was related to magnetic evolution near the filaments. In X-rays, we see the appearance of short, bright structures in the gap between the two parts of the cut inverse *S* that proceed by a few minutes the development of the full uncut inverse *S*. In Hα, we see small spots moving gradually in the gap region during May 7 and 8.

The basic idea is that the full inverse *S* was made of two twisted loops, and that the twist within each of them added to produce an amount of twist in the final structure that exceeded the twist limit for the kink instability. To test the idea, we infer values of the force-free field parameter α in the observed structures by comparing them with models. Then we use the inferred α values to determine the twist in the full inverse *S*.

4.1. *Reconnection and Instability*

Since coronal and chromospheric gas pressures are insignificant compared to their magnetic pressures ($\beta \ll 1$), the magnetic fields must be nearly force-free. However, α is typically not uniform (see Fig. 1 and Paper I), i.e., the extent to

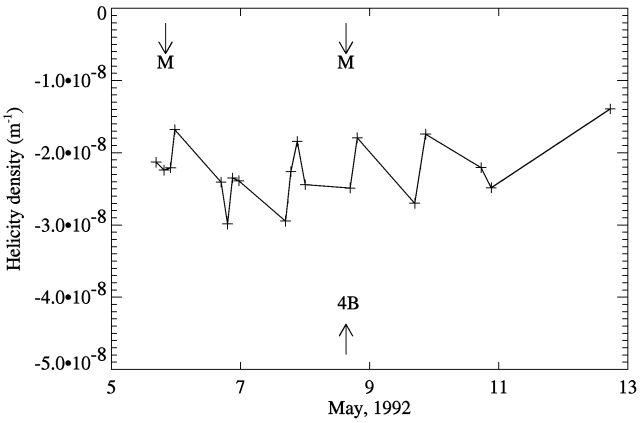

FIG. 4.—Variation of α_{best}, a measure of the average helicity density of the photospheric magnetic field. Arrows indicate start times of Hα (*bottom*) and X-ray flares (*top*), from Solar Geophysical Data. Crosses indicate start times of magnetogram scans.

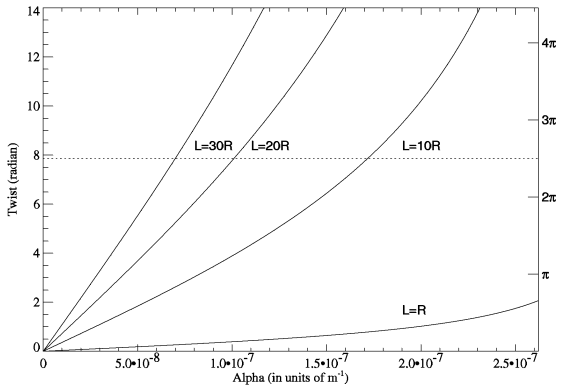

FIG. 6.—Twist of the cylindrical flux tube as a function of the α coefficient of the linear force-free field, computed for flux tube of $R = 10''$ radius. Four curves indicate flux tubes of aspect ratio 1, 10 (*middle*), 20 and 30 (*upper*). Dotted line indicates the 2.5π level of twist.

which the field is twisted varies considerably from one position to another. The largest values of α are many times larger than α_{best}, the best average value given by the procedure discussed above. Using various values of the linear force-free field assumption, α, as well as our vector magnetograms, we determined the value of α that best matches the observed coronal structures. Figures 5*a* and 5*b* show the projected lines of force based on a preflare magnetogram and two values of α, viz., α_{best} and $3\alpha_{best}$. The value $3\alpha_{best}$ gives lines of force similar to the X-ray structures observed before the flare (Figs. 2*b*–2*e*).

It is instructive to study a simplified force-free field model in order to determine whether the amount of twist in the inverse-*S* structure is enough to make it MHD unstable. Consider a cylindrical flux tube having a magnetic field $B = [0, B_\varphi(r), B_z(r)]$, where r is the distance from the axis of the tube. The linear force-free field solution for such a field was given by Lundquist (1951):

$$B_\varphi = B_0 J_1(\alpha r) , \quad (1)$$

$$B_z = B_0 J_0(\alpha r) ,$$

where J_0 and J_1 are Bessel functions. The twist of the tube is

$$\Phi(r) = \frac{LB_\varphi(r)}{rB_z(r)} = \frac{LJ_1(\alpha r)}{rJ_0(\alpha r)} \quad (2)$$

(e.g., Priest 1984), where L is the length of the tube.

Figure 6 shows the relationship between α and the maximum twist (at the outer boundary of the flux tube) for flux tubes of four different lengths and given the radius outer boundary $R = 10''$ computed using equation (2). Obviously, long magnetic flux tubes are more unstable than short ones for a given α value. Now let suppose that the flux tube is linearly stable to kinking if the twist is less than $\Phi_c = 2.5\pi$ (e.g., Hood & Priest 1979). As Figure 6 shows, if we increase the length of the tube, keeping the same helicity density, then the twist will exceed the Φ_c for a tube whose length we can compare to our observations.

From the *Yohkoh* SXT images (Fig. 2), we estimate that the two coronal loops that make up the cut inverse-*S* structure were approximately $230''$ and $110''$ in length. The long single inverse-*S* structure was about $350''$ in length. The smallest loop diameter was about $18''$. For the purpose of discussion, we suppose that the prereconnection coronal loops had radii of $10''$ and aspect ratios of 10 and 20, respectively. Thus, the final loop had an aspect ratio of 30. As Figure 6 shows, after reconnection of these two loops, the final structure will be unstable if the (manifestly stable) individual preflare loops had their respective α values between 7 and 10 in units of 10^{-8} m^{-1}. These are typical local values of the helicity density in this active region (Fig. 1*d*).

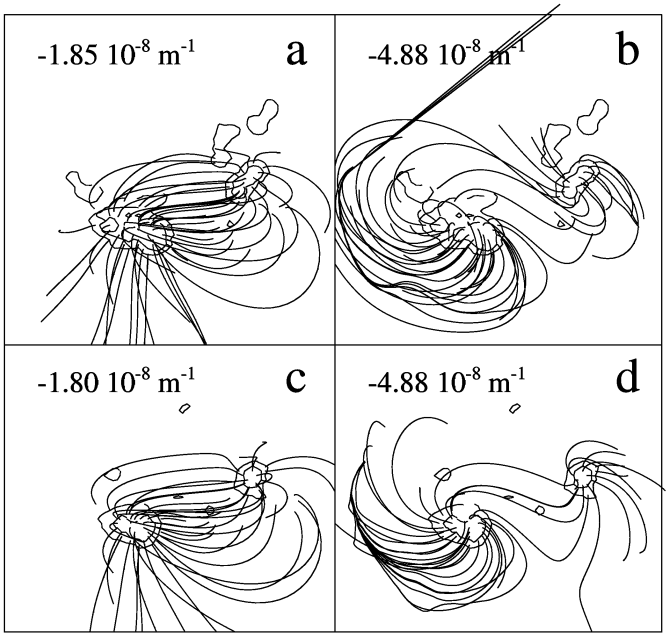

FIG. 5.—Vertical field magnetic contours and projected linear force-free field lines before (*top row*) and after (*bottom row*) the flare for the indicated magnetograms and α values. (*a*) May 7 21:04 UT, $\alpha = -1.85 \times 10^{-8}$ m^{-1}; (*b*) May 7 21:04 UT, $\alpha = -4.88 \times 10^{-8}$ m^{-1}, (*c*) May 9 20:48 UT, $\alpha = -1.80 \times 10^{-8}$ m^{-1}, (*d*) May 9 20:48 UT, $\alpha = -4.88 \times 10^{-8}$ m^{-1}.

5. CONCLUSION

The observations and analysis presented above lead us to believe that the eruption in this region can be understood as a consequence of magnetic reconnection, leading to the MHD kink instability above a twist of about 2π. The observations of Vrsnak et al. (1991) also imply that $\Phi_c \approx 2\pi$.

Theoretical studies imply that this phenomenon cannot be understood adequately in terms of the simple linear theory discussed above (Dahlburg, Antiochos, & Zang 1991). Photospheric field topology plays an important role (Priest 1992), as does magnetic reconnection (Forbes 1992). From a theoretical point of view, the reasons for instability above $\Phi_c \approx 2.5\pi$ are not clear. However, our observations, as well as those of Vrsnak et al. (1991), imply that the Sun takes this value of the critical twist quite seriously. Does twist commonly build up by reconnection? Further studies are required to answer this important question.

We thank the staff of Mees Solar Observatory, who have been supported by NASA grant NAGW-1542 and NASA contract NAS 8-37334, for the observations. The *Yohkoh* Soft X-Ray Telescope is a collaborative project of the Lockheed Palo Alto Research Laboratory, the National Astronomical Observatory of Japan, and the University of Tokyo, supported by NASA and ISAS. This investigation was supported by NSF grant ATM 9303873. Operation of BBSO is supported by NASA through grant NAGW-1972, by the NSF through grant ATM 9320822, and by the ONR through grant N00014-89-J-1069.

REFERENCES

Canfield, R. C., et al. 1993, ApJ, 411, 362
Canfield, R. C., Pevtsov, A. A., & Acton, L. W. 1995, EOS Trans. AGU, Spring Meet Suppl., 76(17), S235
Dahlburg, R. B., Antiochos, S. K., & Zang, T. A. 1991, ApJ, 383, 420
Druzhinin, S. A., Pevtsov, A. A., Levkovsky, V. I., & Nikonova, M. V. 1993, A&A, 277, 242
Feynman, J., & Martin, S. F. 1995, J. Geophys. Res., 100, 3355
Forbes, T. G. 1992, in Lecture Notes in Physics, Vol. 399, Eruptive Solar Flares, ed. Z. Švestka, B. Jackson, and M. Machado (Berlin: Springer), 79
Gary, G. A. 1989, ApJS, 69, 323
Hanaoka, Y. 1994, ApJ, 420, L37
Hood, A. W., & Priest, E. R. 1979, Sol. Phys., 64, 303
Lundquist, S. 1951, Phys. Rev., 83, 307
Mickey, D. L. 1985, Sol. Phys., 97, 223
Moore, R. L., et al. 1980, in Solar Flares: A Monograph from Skylab Solar Workshop II, ed. P. A. Sturrock (Boulder: Colorado Aca. Univ. Press), 341
Moore, R. L., & Roumeliotis, G. 1992, in Lecture Notes in Physics, Vol. 399, Eruptive Solar Flares, ed. Z. Švestka, B. Jackson, & M. Machado (Berlin: Springer), 69
Pevtsov, A. A., Canfield, R. C., & Metcalf, T. R. 1994, ApJ, 425, L117 (Paper I)
———. 1995, ApJ, 440, L109 (Paper II)
Priest, E. R. 1984, Solar Magnetohydrodynamics (Boston: Reidel)
———. 1992, in Lecture Notes in Physics, Vol. 399, Eruptive Solar Flares, ed. Z. Švestka, B. Jackson, & M. Machado (Berlin: Springer), 15
Roumeliotis, G., Sturrock, P. A., & Antiochos, S. K. 1994, ApJ, 423, 847
Shibata, K., et al. 1995, ApJ, 451, L83
Skumanich, A., & Lites, B. W. 1987, ApJ, 322, 473
Solar Geophysical Data. 1992, 579(2), 9
Švestka, Z., & Cliver, E. W. 1992, in Lecture Notes in Physics, Vol. 399, Eruptive Solar Flares, ed. Z. Švestka, B. Jackson, & M. Machado (Berlin: Springer), 1
Tang, F. 1986, Sol. Phys., 105, 399
Tsuneta, S. 1996, ApJ, 456, L63
Tsuneta, S., et al. 1991, Sol. Phys., 136, 37
van Ballegooijen, A. A., & Martens, P. C. M. 1990, ApJ, 361, 283
Vrsnak, B., Ruzdjak, V., & Rompolt, B. 1991, Sol. Phys., 136, 151